Towards modular bone tissue engineering using Ti-Co doped phosphate glass microspheres: cytocompatibility and dynamic culture studies

Carlotta Peticone[1], David da Silva Thompson[1], Gareth Owens[2], HaeWon Kim[3], Martina Micheletti[1], Jonathan C. Knowles[2,3], Ivan B. Wall[2,3].

[1]Department of Biochemical Engineering, University College London, Gordon Street, London WC1E 6BT; [2]Division of Biomaterials and Tissue Engineering, UCL Eastman Dental Institute, Grays Inn Road, London WC1X 8LD; [3]Department of Nanobiomedical Science and BK21 Plus NBM Global Research Center for Regenerative Medicine, Dankook University Graduate School, Cheonan, South Korea

Correspondence:
Ivan Wall
E: i.wall@ucl.ac.uk
T: +44 (0) 207679 9583

Running title: Phosphate glass modular tissue engineering

Keywords: tissue engineering, phosphate glass, titanium, cell culture, bioprocessing, biomaterials

Abstract

The production of large quantities of functional vascularized bone tissue *ex vivo* still represent an unmet clinical challenge. Microcarriers offer a potential solution to scalable manufacture of bone tissue due to their high surface area-to-volume ratio and the capacity to be assembled using a modular approach. Microcarriers made of phosphate bioactive glass doped with TiO_2 have been previously shown to enhance proliferation of osteoblast progenitors and maturation towards functional osteoblasts. Furthemore, doping with cobalt appears to mimic hypoxic conditions that have a key role in promoting angiogenesis. This characteristic could be exploited to meet the clinical requirement of producing vascularized units of bone tissue.

In the current study, the human osteosarcoma cell line MG-63 was cultured on phosphate glass microspheres doped with 5% mol TiO_2 and different concentrations of CoO (0,2 and 5% mol), under static and dynamic conditions (150 and 300 rpm on an orbital shaker). Cell proliferation and the formation of aggregates of cells and microspheres were observed over a period of two weeks in all glass compositions thus confirming the biocompatibility of the substrate and the suitability of this system for the formation of compact micro-units of tissue. At the concentrations tested, cobalt was not found to be cytotoxic and did not alter cell metabolism. On the other hand, the dynamic environment played a key role, with moderate agitation having a positive effect on cell proliferation while higher agitation resulting in impaired cell growth.

Finally, in static culture assays, the capacity of cobalt doping to induce VEGF upregulation by osteoblastic cells was observed, but was not found to increase linearly with CoO content.

In conclusion, Ti-Co phosphate glasses were found to support osteoblastic cell growth and aggregate formation that is a necessary precursor to tissue formation and the upregaulation of VEGF production can potentially support vascularization.

Introduction

Traditional tissue engineering is based on the so called top-down approach, in which cells are first isolated and expanded, and then seeded on a degradable scaffold of predefined size and shape [1]. This is followed by cells spreading homogenously within the scaffold and reassembling the appropriate tissue structure, through secretion of the tissue-specific extracellular matrix. Despite advances in materials development and surface patterning to closely mimic tissue, this type of approach often fails in recreating native tissue microstructures[2]. An alternative approach is modular tissue engineering in which small building blocks of tissue are formed and then assembled into large-scale constructs[1]. Working at the micro-scale enables engineers to recreate original functional units, and unit modules can be created through different methods such as controlled cell aggregation, cell sheet assembly, cell-laden hydrogels or tissue printing [2,3].

A further advantage of the "bottom-up approach" is that during tissue assembly, an interconnected macrostructure is formed that could potentially facilitate *in vivo* vascularization[1]. Furthermore, in regards to bone tissue engineering, a patient-tailored approach could be used, where building blocks are assembled to repair bone defects of specific size and shape, meeting the increasingly common need for personalized medicine.

Microspherical scaffolds have been proposed as a potential modular unit for bone tissue engineering applications[4–6], as their sphericity could facilitate filling of irregular shaped defects [7]. Microspheres have been used both as a tool to expand adherent cells *ex vivo* and also to directly deliver cells to defects to repair or regenerate tissues[8]. While for cell expansion, inert, plastic microcarriers are usually used, microspheres for tissue engineering applications need to be made of a suitable implantable biomaterial that supports cell growth and ideally could direct differentiation towards a specific tissue and promote biological responses *in vivo* [9].

Similar to other types of scaffold, several materials including bioactive ceramics, polymers and their composites have been synthetized in the form of spherical particles and they have been found to support cell attachment to the curved surface, together with growth and differentiation towards an osteogenic phenotype under specific culture conditions [9]. Furthermore, being suitable for integration within a bioreactor system, they are particularly interesting from a bioprocessing perspective as they are easily scalable compared to other types of scaffold.

Bioactive phosphate glass microspheres are appealing potential substrates that will support osteoblastic cell attachment and proliferation. As this material is completely soluble in aqueous media [10], it can be implanted *in vivo* together with cells. Furthermore, the tuneable glass composition can be easily engineered to induce specific structural and biological properties through incorporation of therapeutic ions[11]. For example, titanium and cobalt ions have been shown to induce osteogenesis[6,11] and angiogenesis [12–14], respectively.

In this study, three glass compositions containing 5% mol TiO_2 and different concentrations of CoO (0, 2 and 5% mol) were investigated. The molar concentration of titanium was chosen based

on previous studies, showing cytocompatibility and osteogenic potential of 5% mol TiO_2 doped phosphate glass microspheres [6,15]. As cobalt-induced cytotoxicity has been reported in several studies [16–18], two molar concentrations previously tested in cobalt-releasing bioactive glass scaffold that proved to be safe from a cytotoxic perspective and to promote *in vitro* angiogenesis [12,13] were selected.

Material characterization of all three glass compositions was performed and glass degradation and cobalt release over three weeks was investigated. The osteosarcoma cell line MG-63 was used in all experiments, as this cell line is commonly used in preliminary biocompatibility studies in bone tissue engineering [19].

In these preliminary studies, we sought to investigate whether mixing could enhance cell proliferation on the microspheres compared to static culture. In this work a microwell plate format was used for cell attachment and proliferation experiments, where agitation is achieved by orbital shaking. Mixing and flow characteristics in shaken systems have been studied by Zhang et al. (2005 and 2008), Zhang et al. (2010), Discacciati et al. (2013) and Klöckner & Büchs (2012) among others. Recent work by Weheliye et al. (2013) has demonstrated the presence of two areas, a diffusion-limited area at the bottom of the well and a convection dominated region at the top, the extent of which depends on geometrical ratios and other operating parameters. A flow transition was also reported, corresponding to a critical *Froude* number at which the transition occurs, and the analysis has been extended to two-phase flows in the presence of microcarriers [26]. While their work has been carried out using a well internal diameter d_i = 10 cm (larger than the one employed in this study), the equations can be applied in first approximation to smaller systems to be able to calculate the critical speed at which transition occurs and predict the flow pattern inside the well. Two shaking speeds of 150 and 300RPM were selected in this work as they were lower than the critical speed (N_c = 350RPM) and offered two different mixing patterns to investigate the effect of these on cell proliferation and metabolism.

Cell attachment to the microspheres and cell-microcarrier cluster formation over time were observed through microscopy analysis. Cell proliferation, along with glucose and lactate levels in the culture medium were also tested. Finally, as cobalt was added to the glass composition due to its pro-angiogenic properties, the effect of increasing concentration of Co^{2+} ions on VEGF expression was investigated.

Materials and methods

Glass preparation and microsphere fabrication

Glasses were prepared from the precursors: sodium dihydrogen orthophosphate (NaH_2PO_4), calcium carbonate ($CaCO_3$), phosphorus pentoxide (P_2O_5), titanium dioxide (TiO_2) and cobalt oxide (CoO). All the precursors were obtained from VWR-BDH (Poole, UK). Three different compositions: CoO 0%, CoO 2% and CoO 5% were manufactured as shown in Table 1.

The precursors were weighed and mixed in a Pt/10%Rh crucible (Type 71040, Johnson Matthey, Royston, UK) which was introduced into a preheated furnace (Carbolite, RHF 1500, Sheffield, UK) at 700°C to remove H_2O and CO_2 for 30min. The mixture was then melted at 1300°C for 3 hours. Upon removal from the furnace, the melted glass was quenched onto a steel plate.

The glasses were first broken into fragments and then ball-milled at 10Hz using a Retsch MM301 milling machine (Haan, Germany). The microparticles obtained were then sieved down to 63-106μm (Endecotts Ltd., London, UK) on a Fritsch Spartan sieve shaker (Fritsch GmbH, Idar-Oberstein, Germany). The microparticles were spheroidized by passing them through a flame spheroidization apparatus, as previously described [6].

X-ray diffraction analysis

X-ray diffraction analysis (XRD) was performed using a Bruker- D8 Advance Diffractometer (Bruker, Coventry, UK) in flat plate geometry using Ni filtered Cu Kα radiation. Data was collected at 2θ values ranging from 10° to 100° with a step size of 0.02° and a count time of 12s using a Lynx Eye detector (Bruker).

Differential thermal analysis

Differential thermal analysis (DTA) was carried out using a Setaram Differential Thermal Analyser (Setaram, Caluire, France) to determine the glass transition (T_g), crystallization (T_c) and melting (T_m) temperatures. Powdered glass samples were heated from ambient up to 1000 °C at a heating rate of 20 °C min^{-1} under air purge. Readings were corrected against a blank run.

Fourier transform infrared spectroscopy

Fourier transform infrared spectroscopy was performed on glass powder samples using a Perkin Elmer System 2000 spectrometer (Perkin Elmer, USA) in the range 4000-400 cm^{-1}. Each spectrum was obtained by averaging 10 scans.

Dissolution study

To determine the degradation of the microspheres over time, 250 mg of microspheres were placed in 25ml of deionised water at pH 7. At 0, 1, 3, 7, 14 and 21 days, the solution was removed and stored for further analysis. The microspheres were oven dried and then reweighed and the weight loss

was calculated as a percentage of the original weight. Triplicates of each sample were analysed for each time point.

Cobalt release

The release of cobalt ions from the glasses was studied using a Dionex ICS-2500 ion chromatography system (Dionex, UK), designed for determination of transition and lanthanide metals. Media harvested from the degradation study, containing the released cobalt ions from all the glass compositions, were eluted using an Ion Pac® CS5A cation ion exchange column with attached CG5A guard column. The MetPac® PDCA (Dionex, UK) was used as the eluant concentrate in which pyridine-2,6-dicarboxylic acid (PDCA) functions as a colorimetric complexing agent for metal complex separation via anion exchange. Absorbance was detected at 530nm. The sample run time was set for 10min and each condition was analyzed in triplicates.

Cell culture

The human osteosarcoma cell line MG-63 was used in this study. MG-63 cells were cultured in T-75 tissue culture flasks (Fisher Scientific, Loughborough, UK) with low glucose Dulbecco's Modified Eagle Medium (DMEM), supplemented with 10% fetal bovine serum (FBS) and 1% Antibiotic/Antimycotic (Anti/Anti), all supplied by Life Technologies (Inchinnan, Scotland). Cell cultures were maintained at 37°C/5% CO_2 and passaged every three days using trypsin-EDTA (Life Technologies) solution for 5min at 37°C. Cell number was determined using a Neubauer haemocytometer.

MG-63 expansion on microspheres under static and dynamic conditions

A monolayer of phosphate glass microspheres (5mg/well) was placed into low-adhesion 96-well plate (Corning Costar®, Appleton Woods, Birmingham, UK) in order to prevent cell attachment to the microwell surface. The microspheres were UV sterilized for 90min. MG-63 were seeded on the microspheres at a concentration of 1.5 x 10^4 cells per well and then placed in the incubator at 37°C/5% CO_2 for up to 14 days, with media replaced every two days.

The cell proliferation study was divided into three groups consisting of MG-63 cultures under static conditions and on an orbital shaker at two different speeds, 150 and 300rpm. These speeds were selected based on a experimental fluid dynamic study on cylindrical, orbitally shaken bioreactors [25]. Table 2 summarizes the geometrical characteristics of the experimental system used in this work and the calculated Fr_c and N_c.

As this model is very sensitive on the height of the fluid within the well, two different N_c were computed, based on upper and lower limit of fluid height used in this experimental setting. A range of critical speed between 340-350 RPM was calculated, for well volumes in the range of 150-160µl. Two speeds below N_c, 150 and 300 RPM, were then selected to investigate how mixing conditions would affect cell proliferation and metabolism, however keeping a diffusion limited zone

where the cell-microspheres monolayer is located. A schematic representation of the flow pattern at both the selected speeds and at N_c is given in Figure 1. Cells grown on the orbital shaker were allowed to attach to the microspheres for 24 hrs statically before starting agitation.

Cell staining procedures

Cells were first fixed with 4% paraformaldehyde (PFA) for 10 minutes at room temperature and then washed twice with PBS (1 x 1 min and 1 x 5 min). For F-actin staining, cells were permeabilized with 0.5% Triton X-100 in PBS for 10 min at RT. Cells were stained with Alexa Fluor® 488 phalloidin (1:120 dilution in PBS, Life Technologies) for 20min at RT in the dark. Cells were washed twice with PBS (1 x 1 min and 1 x 5 min). Cells were counter-stained with propidium iodide (PI) (1µg/ml, Sigma, Poole, UK) for 10 min at RT in the dark. Images were obtained using a Radiance 2100 confocal microscope (BioRad, Loughborough, UK).

Cell proliferation assay

Cell proliferation was determined using the Cell Counting Kit-8 (CCK-8, Dojingo, Sigma). Cells were seeded on monolayers of bioactive phosphate glasses (5mg/well) at a concentration of $1.5x10^4$ cells per well and incubated at 37°C/5%CO_2. At different time points, 10µl of CCK-8 reagent was added to each well in the plate and incubate for 2 hours. OD readings were taken at 450nm in a multi-well SafireII plate reader (Tecan, Weymouth, UK). Cell cultured in 96-well plate tissue culture grade plates were used a control. Samples were analysed in triplicates and data presented as mean ± standard variation.

Metabolic profile assay

Glucose and lactate concentration in media collected from cells grown on monolayers of bioactive phosphate glass on low attachment 96-well plate were determined using YSI 2300 STAT Plus analyzer (YSI, Fleet, UK). 50µl of media were collected from each well, centrifuged at 13,000rpm for 30mins to remove any particulates and stored at 4°C until processed. Cells cultured in 96-well tissue culture grade plates were used a control. Triplicates of all conditions were analyzed and the mean ± standard variation was determined.

Human VEGF Immunoassay

A human Quantikine® ELISA assay (R&D Systems, Bio-Techne, Abingdon, UK) was used to detect VEGF levels in cell culture supernatant. A monolayer of phosphate glass microspheres (30mg/well) was placed into low-adhesion 24-well plates (Appleton Woods, UK) and then UV sterilized. MG-63 cells were seeded on the microspheres at a concentration of 9×10^4 cells per well and incubated at 37°C/5%CO_2. Cells grown on standard tissue culture 24-well plates were used as a control. Media was replaced every two days and cell culture supernatant was harvested at 24 and 72hrs post-seeding. Samples of cell culture supernatant were centrifuged at 13,000rpm for 20mins at

4°C and stored at -80°C until processing. The ELISA assay was performed according to manufacturer instructions. The assay was repeated two times and each condition was analysed in duplicates. Data are presented as mean ± standard variation (n=4).

Statistical analysis

All data are shown as mean ± standard deviation, if not differently stated.

Statistical signifiance was assessed via a two-way ANOVA followed by Bonferroni's multiple comparison test (significance level ≤ 0.05), using GraphPad Prism software (GraphPad, USA), as reported per experiment.

Results

X-Ray Diffraction Analysis

The XRD spectra are shown in Appendix 1 (Fig. A.1). No crystalline phases were detected and a broad peak was observed at values of 2θ between 20-40° for all compositions, confirming the glassy nature of the samples.

Fourier Transform Infrared Spectroscopy

FTIR was used to determine any changes in chemical groups present in the glass structure, due to doping with metal oxides. In particular, the effect of increasing molar concentration of Co^{2+} on PO^{2-}, PO_3^{2-} and P-O-P groups was analysed.

In accordance to previous studies [12,27,28], peaks in the spectra were assigned as follows:

- the absorption bands at 1260-1270 cm^{-1} correspond to asymmetric stretching of PO^{2-};
- the absorption bands at 1100 and 1000 cm^{-1} are assigned to the asymmetric and symmetric stretching of PO_3^{2-} respectively;
- the absorption bands at 890 and 730 cm^{-1} correspond to the asymmetric and symmetric P-O-P respectively.

Similar to what was shown by Lee et al. (2013), there was a reduction in intensity of the bands with increasing Co^{2+} content (Appendix 1, Fig. A.2). Furthermore, a shift towards higher energy is observed for the PO^{2-} band, with increasing Co^{2+} content.

Differential Thermal Analysis

DTA was used to determine the glass transition (T_g), crystallization (T_c) and melting temperatures (T_m). T_g, T_c and T_m from Figure A.3 (Appendix 1) are summarized in Table A.1 (Appendix 1). No significant changes in T_g and T_c were noticed between the three glass compositions. Two crystallization peaks were noticed for all glass compositions, together with a reduction in size in the T_m peak with increasing Co^{2+} content, confirming results previously seen by Lee et al. (2013). Furthermore, T_m was found to be inversely proportional to Co^{2+} content.

Dissolution study and cobal release

In the dissolution study, weight loss of the glass samples was assessed as a function of time (Fig. 2.a). The dissolution rate clearly decreased with increasing cobalt content within the glass. Dissolution of cobalt-free glass was considerably faster than the other two compositions, showing a 24.5% (± 2.0%) weight loss at 21 days, compared to 18.7% (± 0.6%) and 17.5% (± 1.6%) of CoO 2% and 5% respectively. Dissolution rates are shown and were calculated as the slope of the regression line plotted for each composition.

Cumulative cobalt ion release from all three glass compositions over a period of 21 days was determined (Fig. 2.b). Co^{2+} ion release from CoO 5% microspheres was consistently higher than CoO 2% throughout the period analysed. At day 3, the concentration of Co^{2+} ions released by CoO 5% (8.68 ±0.20 ppm) was approximately three-fold higher than that of CoO 2% (3.27 ±0.17 ppm).

MG-63 culture on bioactive glass microspheres

The MG-63 cell line was successfully cultured on a layer of phosphate bioactive glass microspheres over a period of 13 days. Cell attachment and growth were observed on all three glass compositions, Co0%, Co2% and Co5%. Cell attachment to the microspheres was evident from the first day of culture under static conditions (Fig. 3). After one week of culture, bridging of microspheres by cells became evident and the formation of clusters occurred. By the end of the two week culturing period, the formation of a single network of microspheres was observed.

The formation of 3D clusters was also observed using confocal microscopy at day 13 (Fig. 4). Actin filaments in the cytoskeleton were stained using Alexa fluor® 488 phalloidin. Nuclei were stained red using propidium iodide. Single or multi-layers of cells wrapped around the microspheres were clearly observed.

Cell proliferation and metabolic profile

Growth curves for MG-63 cells cultured on monolayers of phosphate glass microspheres were generated for all three different glass compositions under static culure and dynamic (150 rpm and 300 rpm) conditions. The concentration of cobalt tested did not have any adverse effect on cell proliferation; and comparable levels of expansion were obtained for all three substrates (~4.0×10^4 cells after two weeks of culture, $p>0.05$) (Fig. 5). On the other hand, the dynamic environment was found to have a significant impact on cell proliferation (Fig. 6). For all glass compositions, cells cultured under static conditions or on the rotary shaker at 150 rpm exhibited similar behaviour. A detrimental reduction in cell number at 300 rpm occurred 48 hours from the start of agitation and the number of cells seemed to plateau from day 5 to the end of the culture.

Furthermore, in both static and 150rpm, nearly all microspheres were colonized by cells by the end of the two weeks culturing period and the formation of a single cluster was observed at day 13

(Fig. 7). A small percentage of cell-free microspheres was observed at 150rpm, thus suggesting higher cell expansion per surface area than in static conditions, however, at 300rpm, the formation of aggregates of carriers was less evident, and at day 13, a large surface area was still populated by cell-free microspheres. This was reflected in the growth curve data in Fig. 6, showing inhibited cell growth throughout the timeframe analysed, independently of the glass composition.

At the same time, glucose consumption and lactate production profiles also mapped to, and reflected differences in, proliferation rates. For all glass compositions, static and 150 rpm conditions resulted in the highest rate of glucose consumption and lactate production; whereas 300 rpm conditions gave rise to the lowest and was significantly lower compared to static ($p<0.05$, starting from day 5 for all glass compositions), thus confirming limited growth under this condition (Fig. 8.

Next, the yield of lactate produced from glucose consumed ($Y_{lactate/glucose}$) (which indicates the rate of glycolysis) was characterized for all three compositions and for the tissue culture plastic control, in both static and 150 RPM conditions (Fig. 9). As expected, $Y_{lactate/glucose}$ for the control stabilized at a value of ~2 from day 3 of culture. Cells grown on CoO 0% and 2% microspheres presented a higher ratio up to day 3 under static conditions that corresponded to the limited growth observed during early days of culture. From day 5, overlapping between the curves corresponding to the cells grown on the microspheres and the control was observed ($p>0.05$). For the CoO 5% microspheres, overlapping was observed starting from day 7. At 150 rpm, no significant differences between culture on the phosphate glass microspheres and the control were observed from day 3 ($p>0.05$).

Human VEGF Immunoassay

The concentration of VEGF (mg/ml/cell) in supernatant, secreted by MG-63 cells under static conditions for all three glass compositions was measured (Fig. 10). Cells grown in planar standard tissue culture plastic were used as a negative control. In all conditions, VEGF expression was found to increase with time, with higher concentrations observed after three days of culture. Significantly higher levels of expression were observed for cells cultured on the cobalt-doped microspheres at both time points. At day 1, however, Co-induced VEGF secretion was not found to be significantly higher than the control conditions ($p>0.05$). At day 3, VEGF secretion on both Co-doped microspheres was found to be significantly higher than in CoO 0% and the plastic control. Highest expression was observed on CoO 2% after 72 hours of culture (0.045±0.026 pg/ml/cell). Interestingly, VEGF expression by cells cultured on CoO 5% microspheres was significantly lower than CoO 2% ($p<0.05$). The cobalt free glass and plastic control displayed a similar behaviour, with minimal VEGF expression at both time points.

Discussion

Phosphate glasses have been identified suitable biomaterials for bone tissue engineering applications [10,29]. Key features of these materials are their capacity to be fully resorbed and the versatility of their structure to incorporate therapeutic ions[11]. Thanks to these characteristics, phosphate bioactive glasses can be classified as a "third generation biomaterial", meaning that the implant is not only temporary, but plays an active role in the regeneration of the damaged tissue [10].

In this study, phosphate bioactive glass microspheres were doped with TiO_2 and CoO, due to their osteogenic [30–33] and angiogenic properties respectively [12,13,34]. Physical characterization of the material was firstly performed. Biocompatibility, cell attachment, proliferation and metabolite production by a human osteoblastic cell line when grown on the phosphate glass microspheres were then investigated.

Binary doping with cobalt and titanium had a significant effect on microsphere degradation. In CoO 0%, 25% weight loss occurred in a period of three weeks, while the weight loss was reduced by approximately 20% for compositions containing cobalt. Dissolution followed a linear trend during the three week period analyzed. The actual rate of dissolution when cells are introduced and in physiologic conditions would likely be slower because phosphate glass degradation in acellular simulated body fluid (SBF) occurs at a slower rate[35].

All three glass compositions were found to be biocompatible and were able to support cell attachment and proliferation. Moreover, the different concentrations of cobalt tested did not have a negative effect on cell expansion capacity. This result was particularly relevant, as cobalt induced toxicity has been reported from wear, corrosion and leaching of CoCr implants *in vivo* [36], due to oxidative damage to cells by reactive oxygen species (ROS) [18], causing DNA strand breaks and oxidation of bases. Comparable trends in cell proliferation were observed on all substrates. This is likely due to the slow controlled release of cobalt ions by the phosphate glass microspheres. Fleury et al. (2006) reported a decrease in MG-63 cell number when exposed to 2.5-10 ppm Co^{2+} ions in a dose dependent manner. Similarly, Wu et al. (2012) reported a slight decrease in cell number on BM-MSCs grown on 5% cobalt doped mesoporous bioactive scaffold. However, in a previous study using Ti-Co-doped phosphate glass discs for MG-63 culture, 5% mol CoO was identified as the cytotoxicity safety threshold [12]. In this work, Co^{2+} ions released in deionised water by CoO 5% microspheres over three days (the interval used for media exchange was of two days) corresponds to approximately 8.7 ppm. However, as the actual concentration sensed by cells is lower than that detected in deionised water, this explains the lack of cytotoxicity observed even at the highest cobalt concentration.

The formation of a 3D network, by bridging together of adjacent cells, was also observed. However, not all the cells directly attached to the surface of the microspheres; instead cell-to-cell attachment also occurred. Since the microspheres were not biofunctionalized in this study, surface coating could represent a potential strategy to increase cell adherence to the microspheres and to promote growth. Indeed, modifications in surface chemistry [37], topography [32,38] and tethering of fusion

proteins [39] have all been identified as successful strategies to biofunctionalize biomaterials for bone tissue engineering. The formation of these aggregates of cells and carriers potentially lends itself to a bottom-up approach, in which micro-units of tissue are created separately and are then fused together to produce large, even custom-shaped pieces of tissue at the point of delivery, rather than the traditional approach that defines the scaffold shape prior to seeding cells.

The capacity of cobalt to enhance VEGF expression was also confirmed, supporting other's observations that Co^{2+} ions can induce hypoxia-like responses in cells [12–14,34] by stabilization of the α-subunits of the HIF transcription factors [40]. In this study, the concentration of VEGF in culture was higher in cells grown on microspheres containing cobalt than in the Co-free microspheres. Cobalt-free microspheres performed similarly to the plastic control showing minimal level of VEGF secretion. Despite higher Co^{2+} ion release being observed in the CoO 5% composition, this did not correspond to a relative increase in VEGF production, but rather a reduction in expression compared to CoO 2%. This was in line with previous observations showing no direct correlations between increasing CoO molar concentration and VEGF secretion[12]. Wu et al. (2012) showed enhanced VEGF gene expression and HIF-1α expression by bone marrow MSCs cultured on mesoporous bioactive glass scaffold doped with 5% mol CoO in comparison to 2% mol scaffold, however, even in their study, this did not translate into enhanced VEGF secretion in the media.

Mixing was found to have a critical effect on cell proliferation. Weheliye et al. (2013) previously showed how to characterize flow and mixing dynamics in a cylindrical shaken bioreactor. They observed a mixing pattern characterized by the formation of two counter-rotating toroidal vortices. At low shaking frequency, the formation of two distinct zones within the reactor was observed. A first zone, close to the free surface, was dominated by convection, while a second zone, close to the bottom of the plate, below the vortical structures, was dominated by diffusion. As the shaking frequency *N* was increased, the size and magnitude of the vortices increased, until extending over the entire height of the cylinder, thus dominating the flow conditions within the reactor. At higher rotational speed the flow pattern changed, with the vortices rotating in opposite direction compared to the movement of the system. This "out of phase" phenomenon was found to start at a specific critical shaking frequency, *Nc*. For this system, *Nc* was determined and found to be equal to 350rpm. Two rotational speeds, both of which were lower than *Nc* where then selected and investigated.

Mild agitation at 150rpm promoted cell proliferation, with cells reaching approximately a four fold increase (between 5.2- 5.7 x 10^4 cells for all glass compositions) in number after approximately nine days in culture, before plateauing. Compared to static culture, agitation at 150rpm performed better towards the second half of the culturing period, although this effect was not found to be statistically significant. When the culture plates were shaken at the higher agitation rate of 300rpm, a detrimental effect on cell growth was observed. The formation of clusters was inhibited and by the end of the culturing period, a large majority of carriers was not colonized by cells. On the other hand,

colonization of the totality of carriers by cells occurred under static conditions. At 150rpm, despite the highest cell yield, a small percentage of cell-free microspheres was present, thus suggesting that a higher cell/surface ratio was obtained at this dynamic condition.

Metabolic data showing lactate production and glucose in the supernatant correlate with trends observed in the growth curves. Higher lactate production and glucose uptake was observed at 150rpm, followed by static culture and with minimum glucose consumption observed at 300rpm, correlating to the limited growth observed. Enhanced mixing conditions with more homogenous distribution of nutrients and oxygen within the well could be responsible for the general improvement in cell proliferation observed at 150rpm. The metabolic analysis was particularly relevant to understand whether cobalt-induced hypoxia or 3D culture could have an effect on cell metabolism, as post-translational stabilization of the hypoxia-inducible transcription factor HIF-1α has been reported to upregulate the rate of glycolysis [41]. In particular, $CoCl_2$ (100μM) induced hypoxia has been reported to cause a metabolic switch in hMSCs, in terms of increased lactate release and impaired oxygen consumption rate[42]. Furthermore, this was found to inhibit the capacity of hMSCs to undergo osteogenic differentiation. For this experiment, cells grown on tissue culture plastic in 2D monolayer were used a control. The theoretical lactate to glucose $Y_{lactate/glucose}$ ratio is ~ 2 [43,44], with higher values usually associated with anaerobic metabolism. It was found that $Y_{lactate/glucose}$ stabilized at a value of ~2 after 72 hours of culture for the control, while an initial higher ratio was observed on all phosphate glass microspheres. However, the $Y_{lactate/glucose}$ eventually stabilized around 2 from the day 5 for CoO 0% and 2% and starting from day 7 for CoO 5%, under static culture. Under dynamic conditions, no significant differences between the control and all microspheres were observed starting from day 3. Thus, cobalt-doping at the concentrations tested did not have a significant impact on cellular metabolism.

Ti/Co doped phosphate glass microspheres represent a suitable substrate for the expansion of cells of osteoblastic origin. The formation of a 3D network of clusters suggest that cells are able to create a suitable microenvironment when cultured on this type of material. Furthermore, the aggregation effect could be exploited to form tailored micro-units of bone tissue to be used for bone regeneration purposes.

The importance of dynamic culture conditions was clearly shown. When increasing the shaking speed, cell growth was inhibited as well as the clustering effect. As the rotation speed increases, larger toroidal vortices start forming within the well, leading to an increase in size of the convection dominated region [45]. This might interfere with the microcarrier/cell monolayer, thus inhibiting growth, colonization of cell-free microspheres and cluster formation. A suitable reactor system, in which cells can be exposed to optimal mixing conditions and at the same time be kept packed to favour the formation of clusters and the colonization of cell-free carriers, should be investigated.

Compared to commercially available microspheres, those analyzed in this study present the advantage of being fully resorbable, thus simplifying the bioprocessing sequence if applying the cells in a tissue engineering application, as a harvesting step is not required after expansion. Furthermore, the combined properties of titanium and cobalt are particularly promising for bone regeneration. From this preliminary study, cobalt doping did not have a negative effect on cell growth and comparable proliferation was noticed on all compositions. In terms of VEGF production, the increase in cobalt concentration did not translate in more VEGF being secreted, similarly to what observed in previous studies [12,13]. Thus, keeping the cobalt content to a minimum value of 2% is sufficient to simulate a hypoxic state and to promote angiogenic responses. However, it is essential to determine whether this translates into functional outputs such as promoting endothelial cells proliferation and vessel formation, *in vitro* and *in vivo* and to test the effect of binary doping on osteodifferentiation.

Conclusion

Phosphate bioactive glass microspheres doped with titanium and cobalt were shown to be a biocompatible substrate for osteoblastic cells. Cobalt was found not to be cytotoxic at the concentration tested and successful growth of a model human cell line was obtained on all glass compositions.

The fluid dynamic environment played a key role in cell growth and metabolism. Improved cell growth was obtained when growing the cells at a moderate shaking frequency. The dynamic data suggest that a bioreactor configuration, able to provide the required mixing environment and to promote cells clustering, should be identified and investigated. For example, a perfusion bioreactor, where microspheres and cells can be packed together and exposed to continuous perfusion, offers an ideal set-up for this particular system.

The capacity of cobalt-doped microspheres to enhance VEGF secretion was also demonstrated, although this effect was not found to be directly dependent on cobalt concentration. However, the angiogenic potential of this substrate should be further investigated by assessing functional outcomes such as sprouting and capillary tube formation by endothelial cells.

References

1. Mei, Y. *et al.* Modulating and modeling aggregation of cell-seeded microcarriers in stirred culture system for macrotissue engineering. *J. Biotechnol.* **150,** 438–446 (2010).

2. Nichol, J. W. & Khademhosseini, A. Modular tissue engineering: engineering biological tissues from the bottom up. *Soft Matters* **5,** 1312–1319 (2010).

3. Liu, J. S. & Gartner, Z. J. Directing the assembly of spatially organized multicomponent tissues from the bottom up. *Trends in Cell Biology* **22,** 683–691 (2012).

4. Hong, S. J., Yu, H. S. & Kim, H. W. Preparation of porous bioactive ceramic microspheres and in vitro osteoblastic culturing for tissue engineering application. *Acta Biomater.* **5,** 1725–1731 (2009).

5. Chan, B. P., Hui, T. Y., Wong, M. Y., Yip, K. H. K. & Chan, G. C. F. Mesenchymal stem cell-encapsulated collagen microspheres for bone tissue engineering. *Tissue Eng. Part C. Methods* **16,** 225–235 (2010).

6. Lakhkar, N. J. *et al.* Titanium phosphate glass microspheres for bone tissue engineering. *Acta Biomater.* **8,** 4181–90 (2012).

7. Perez, R. A., Riccardi, K., Altankov, G. & Ginebra, M.-P. Dynamic cell culture on calcium phosphate microcarriers for bone tissue engineering applications. *J. Tissue Eng.* **5,** 1–10 (2014).

8. Martin, Y., Eldardiri, M., Lawrence-Watt, D. J. & Sharpe, J. R. Microcarriers and their potential in tissue regeneration. *Tissue Eng. Part B. Rev.* **17,** 71–80 (2011).

9. Park, J.-H. *et al.* Microcarriers designed for cell culture and tissue engineering of bone. *Tissue Eng. Part B. Rev.* **19,** 172–90 (2013).

10. Knowles, J. C. Phosphate based glasses for biomedical applications. *J. Mater. Chem.* **13,** 2395 (2003).

11. Lakhkar, N. J. *et al.* Bone formation controlled by biologically relevant inorganic ions: Role and controlled delivery from phosphate-based glasses. *Adv. Drug Deliv. Rev.* **65,** 405–20 (2013).

12. Lee, I.-H. *et al.* Development, characterisation and biocompatibility testing of a cobalt-containing titanium phosphate-based glass for engineering of vascularized hard tissues. *Mater. Sci. Eng. C* **33,** 2104–2112 (2013).

13. Wu, C. *et al.* Hypoxia-mimicking mesoporous bioactive glass scaffolds with controllable cobalt ion release for bone tissue engineering. *Biomaterials* **33,** 2076–2085 (2012).

14. Azevedo, M. M. *et al.* Hypoxia Inducible Factor-Stabilizing Bioactive Glasses for Directing Mesenchymal Stem Cell Behavior. *Tissue Eng. Part A* **21,** 382–389 (2015).

15. Guedes, J. C. *et al.* TiO(2)-doped phosphate glass microcarriers: a stable bioactive substrate for expansion of adherent mammalian cells. *J. Biomater. Appl.* **28,** 3–11 (2013).

16. Catelas, I., Petit, A., Zukor, D. J. & Huk, O. L. Cytotoxic and apoptotic effects of cobalt and chromium ions on J774 macrophages - Implication of caspase-3 in the apoptotic pathway. *J. Mater. Sci. Mater. Med.* **12,** 949–953 (2001).

17. Fleury, C. *et al.* Effect of cobalt and chromium ions on human MG-63 osteoblasts in vitro: Morphology, cytotoxicity, and oxidative stress. *Biomaterials* **27,** 3351–3360 (2006).

18. Simonsen, L. O., Harbak, H. & Bennekou, P. Cobalt metabolism and toxicology-A brief update. *Sci. Total Environ.* **432,** 210–215 (2012).

19. Clover, J. & Gowen, M. Are MG-63 and HOS TE85 human osteosarcoma cell lines representative models of the osteoblastic phenotype? *Bone* **15,** 585–591 (1994).

20. Zhang, H., Williams-Dalson, W., Keshavarz-Moore, E. & Shamlou, P. A. Computational-fluid-dynamics (CFD) analysis of mixing and gas-liquid mass transfer in shake flasks. *Biotechnol. Appl. Biochem.* **41,** 1–8 (2005).

21. Zhang, H., Lamping, S. R., Pickering, S. C. R., Lye, G. J. & Shamlou, P. A. Engineering characterisation of a single well from 24-well and 96-well microtitre plates. *Biochem. Eng. J.* **40,** 138–149 (2008).

22. Zhang, X. *et al.* Use of orbital shaken disposable bioreactors for mammalian cell cultures from the milliliter-scale to the 1,000-liter scale. *Adv. Biochem. Eng. Biotechnol.* **115,** 33–53 (2010).

23. Discacciati, M. *et al.* Numerical simulation of orbitally shaken viscous fluids with free surface. *Int. J. Numer. Methods Fluids* **71,** 294–315 (2013).

24. Klöckner, W. & Büchs, J. Advances in shaking technologies. *Trends in Biotechnology* **30,** 307–314 (2012).

25. Weheliye, W., Yianneskis, M. & Ducci, A. On the fluid dynamics of shaken bioreactors-flow characterization and transition. *AIChE J.* **59,** 334–344 (2013).

26. Pieralisi, I., Rodriguez, G., Micheletti, M., Paglianti, A. & Ducci, A. Microcarriers' suspension and flow dynamics in orbitally shaken bioreactors. *Chem. Eng. Res. Des.* **108,** 198–209 (2016).

27. Abou Neel, E. A. *et al.* Structure and properties of strontium-doped phosphate-based glasses. *J. R. Soc. Interface* **6,** 435–446 (2009).

28. Lakhkar, N. J. Phosphate Glass Microspheres as Cell Microcarrier Substrates for Bone Tissue Engineering Applications. (University College London, 2014).

29. Brauer, D. S. in *Bio-Glasses: An Introduction* (eds. Jones, J. R. & Clare, A. G.) (John Wiley & Sons Ltd, 2012).

30. Abou Neel, E. A. *et al.* In vitro bioactivity and gene expression by cells cultured on titanium dioxide doped phosphate-based glasses. *Biomaterials* **28,** 2967–77 (2007).

31. Abou Neel, E. A. & Knowles, J. C. Physical and biocompatibility studies of novel titanium dioxide doped phosphate-based glasses for bone tissue engineering applications. *J. Mater. Sci. Mater. Med.* **19,** 377–386 (2008).

32. Wall, I., Donos, N., Carlqvist, K., Jones, F. & Brett, P. Modified titanium surfaces promote accelerated osteogenic differentiation of mesenchymal stromal cells in vitro. *Bone* **45,** 17–26 (2009).

33. Kiani, A. *et al.* Titanium-containing bioactive phosphate glasses. *Philos. Trans. R. Soc. A Math. Phys. Eng. Sci.* 1352–1375 (2012). doi:10.1098/rsta.2011.0276

34. Quinlan, E. *et al.* Hypoxia-mimicking bioactive glass/collagen glycosaminoglycan composite scaffolds to enhance angiogenesis and bone repair. *Biomaterials* **52,** 358–366 (2015).

35. Navarro, M. *et al.* Physicochemical Degradation of Titania-Stabilized Soluble Phosphate Glasses for Medical Applications. *J. Am. Ceram. Soc.* **86,** 1345–1352 (2003).

36. Bose, S., Fielding, G., Tarafder, S. & Bandyopadhyay, A. Trace element doping in calcium phosphate ceramics to understand osteogenesis and angiogenesis. *Trends Biotechnol* **18,** 1199–1216 (2013).

37. Mitra, J., Tripathi, G., Sharma, A. & Basu, B. Scaffolds for bone tissue engineering: role of surface patterning on osteoblast response. *RSC Adv.* **3,** 11073 (2013).

38. Brett, P. M. *et al.* Roughness response genes in osteoblasts. *Bone* **35,** 124–133 (2004).

39. Lee, J. H. *et al.* Tethering bi-functional protein onto mineralized polymer scaffolds to regulate mesenchymal stem cell behaviors for bone regeneration. *J. Mater. Chem. B* **1,** 2731 (2013).

40. Yuan, Y., Hilliard, G., Ferguson, T. & Millhorn, D. E. Cobalt inhibits the interaction between hypoxia-inducible factor- and von Hippel-Lindau protein by direct binding to hypoxia-inducible factor-a. *J. Biol. Chem.* **278,** 15911–15916 (2003).

41. Lum, J. J. *et al.* The transcription factor HIF-1alpha plays a critical role in the growth factor-dependent regulation of both aerobic and anaerobic glycolysis. *Genes Dev.* **21,** 1037–1049 (2007).

42. Hsu, S.-H., Chen, C.-T. & Wei, Y.-H. Inhibitory effects of hypoxia on metabolic switch and osteogenic differentiation of human mesenchymal stem cells. *Stem Cells* **31,** 2779–88 (2013).

43. Wagner, R. in *Mammalian Cell Biotechnology in Protein Production* (eds. Hauser, H. & Wagner, R.) (Walter de Gruiter, 1997).

44. Higuera, G. a *et al.* Patterns of amino acid metabolism by proliferating human mesenchymal stem cells. *Tissue Eng. Part A* **18,** 654–64 (2012).

45. Weheliye, W., Yianneskis, M. & Ducci, A. On the Fluid Dynamics of Shaken Bioreactors — Flow Characterization and Transition. **00,** 1–11 (2012).

Figure Legends:

Figure 1: Schematic representation of mixing conditions in a 96 well plate at different shaking speed. At 150RPM, a distinction between the convective (top, red) and diffusive (bottom, pink) area is clearly observed. At 300 RPM, a reduction in size of the diffusion- dominated area is observed, with vortices increasing in size. At 350RPM, when the critical shaking frequency is reached, convection dominates the flow within the well.

Figure 2: a) Dissolution profile for all three phosphate glass compositions, represented as percent cumulative weight loss as a function of time. Measurements were performed in triplicate at each time point and data are shown as mean ± standard deviation; b) Cumulative Co^{2+} ion release presented as ppm g^{-1} as a function of time under static conditions. Measurements were performed in triplicate at each time point and data are shown as mean ± standard deviation.

Figure 3: Phase contrast microscopy images showing MG63 culture on microspheres and cluster formation as a function of time on CoO 2% (A) and CoO 5% (B) microspheres. Scale bar 10x 400µm, 20x 200 µm, 4x 1000µm.

Figure 4: Confocal images of MG63 cultured on phosphate glass microspheres. Nuclei are shown in red and the cytoskeleton in green. Images were obtained at 20x magnification.

Figure 5: Growth curve of MG-63 cultured on phosphate glass microspheres over 13 days of static culture. Growth occurred on all phosphate glass compositions and cobalt doping did not have an effect on cell expansion at the concentrations tested. Each condition was repeated in triplicate and data are presented as mean ± standard deviation. Statistical significance was assessed using a 2-way ANOVA following Bonferroni post test, $p>0.05$ at all time points.

Figure 6: Growth curves for all three phosphate glass microspheres compositions (○ CoO 0%, □ CoO 2% and Δ CoO 5%) and culture conditions. Overlapping between growth curves of cells cultured on different microspheres, under the same dynamic environment, clearly shows the significant effect of mixing on cell growth. Overlapping between static culture (black curves) and 150 RPM (blue curves) is observed over time No significant differences between these two conditions were observed ($p>0.05$ at all time points). At 300 RPM (red curves), a significant decrease in cell number is observed after the start of the agitation regime and impaired cell growth is observed throughout the two weeks of culture. Significant differences in cell number ($p<0.05$) were observed starting from day 5 between 300rpm and the static control for all conditions. Each condition was repeated in triplicates and data are presented as mean ± standard deviation. Statistical significance was assessed using a 2-way ANOVA following Bonferroni post test, by comparing all three microsphere compositions against the control at each time point.

Figure 7: Effect of different dynamic conditions on cell clustering over a two week culturing period. At day 3, a monolayer of microspheres can be observed in all three conditions. After one week in culture, the formation of cell-microsphere clusters is evident and in static culture and at 150 RPM, only half of the surface of the well is occupied by the microspheres. A similar trend is observed at the end of the culturing period in both conditions. However, at 150 RPM, the presence of a small percentage of cell-free microspheres is noticed. At 300 RPM, no changes are observed between day 3 and day 13, with microspheres being still arranged in a monolayer and presenting limited clustering. Scale bar 2000μm.

Figure 8: Lactate production and glucose consumption as a function of time of MG-63 cultured on phosphate glass microspheres statically or at different agitation regimes (150 and 300RPM). Overlapping between glucose consumption and lactate production curves are observed for all microsphere compositions in static culture and at 150 RPM ($p>0.05$). Significantly reduced glucose consumption and lactate production is observed at 300RPM compared to static culture, matching the limited growth observed. Each condition was analysed in triplicates and data are presented as the mean ± standard deviation. Statistical significance was determined using a two-way ANOVA followed by Bonferroni post-test, by comparing all three microsphere compositions against the control at each time point.

Figure 9: Lactate (mmol/L/cells) to glucose (mmol/L/cells) ratio of MG-63 cultured on phosphate glass microspheres under static condition or at 150RPM. Cells grown on standard tissue culture plastic were used as a control. Under static conditions, $Y_{lac/gluc}$ was found to be higher than the control at day 1 and 3 for all phosphate glass microspheres ($p<0.05$) and at day 5 for CoO 5% ($p<0.001$). However, no significant differences were observed after these time points ($p>0.05$). At 150 rpm, statistical significance between the phosphate glass microspheres and the control was reported only at day 1 ($p<0.01$). Data are shown as mean ± standard deviation. Statistical significance was determined using a two-way ANOVA followed by Bonferroni's multiple comparison post-test, by comparing all three microsphere compositions against the control at each time point.

Figure 10: VEGF expression of MG-63 grown on phosphate glass microspheres. VEGF concentration in the supernatant was normalized per cell number. Cells grown on tissue culture plastic were used as a control. Pooled data from two repeated experiments are presented and data are shown as mean ± standard deviation, n=4. Statistical significance was determined using a 2-way ANOVA followed by Bonferroni's multiple comparison test, *$p>0.05$, ** $p<0.01$, *** $p<0.001$.

Appendix

Figure A.1: X-ray diffraction spectra of phosphate glass containing 0%, 2% and 5% mol CoO

Figure A.2: FTIR spectra of phosphate glass containing 0%, 2% and 5% mol CoO.

Figure A.3: Differential Thermal Analysis spectra for phosphate glass containing 0%, 2% and 5% mol CoO. Glass transition temperature (T_g), crystallization temperature (T_c) and melting temperature (T_m) are shown in the graph.

Glass Code	Glass composition (mol%)				
	P_2O_5	CaO	Na_2O	Ti_2O	CoO
CoO %	45	30	20	5	0
CoO 2%	45	28	20	5	2
CoO 5%	45	25	20	5	5

Table 1: Summary of glass compositions, showing molar concentration of precursors.

		96 well plate	Unit
Well inner diameter	d_i	0.0064	m
Orbital diameter	d_o	0.01	m
Liquid volume (min)	Vl_{min}	0.00000015	m^3
Liquid volume (max)	Vl_{max}	0.00000016	m^3
Critical Froude number (min)	Fr_{cmin}	0.65	
Critical speed (min)	N_{cmin}	340	min^{-1}
Critical Froude number (max)	Fr_{cmax}	0.70	
Critical speed (max)	N_{cmax}	350	min^{-1}
Selected speed 1	N_1	150	min^{-1}
Selected speed 2	N_2	300	min^{-1}

Table 1: Summary of geometrical characteristics and calculated Fr_c and N_c (at minimum and maximum operating volume) for the experimental system. Speeds selected for investigation are also reported.

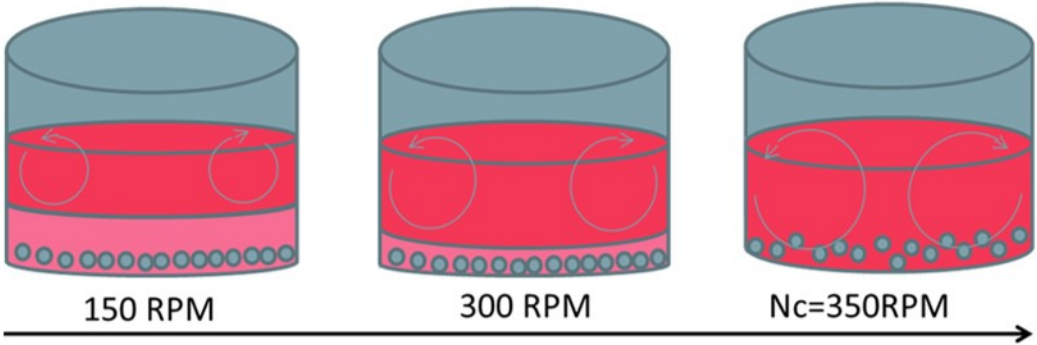
150 RPM
300 RPM
Nc=350RPM
Rotational Speed

a

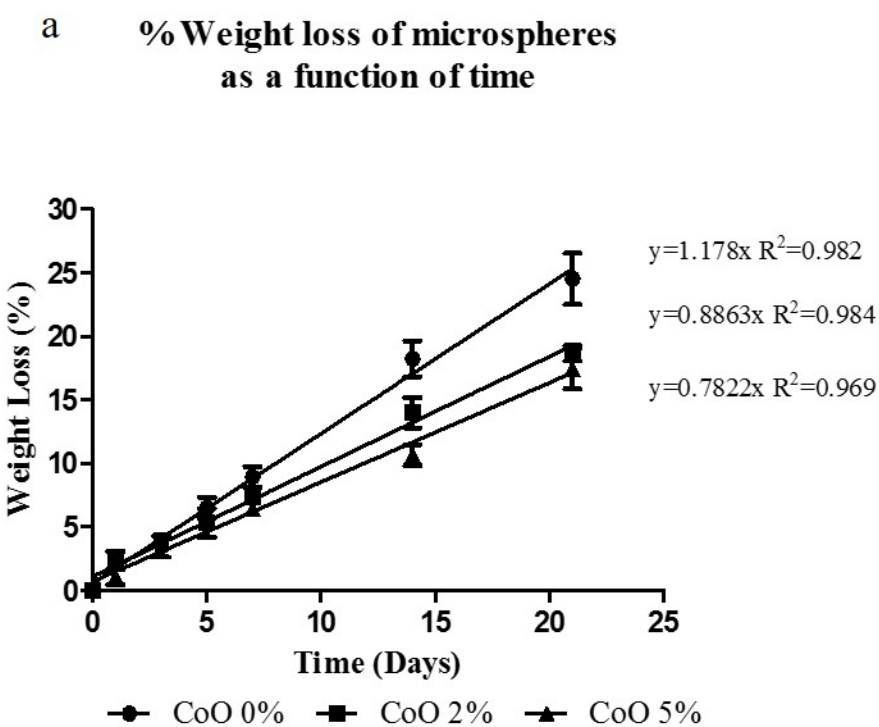
% Weight loss of microspheres as a function of time
Weight Loss (%)
Time (Days)
y=1.178x R2=0.982
y=0.8863x R2=0.984
y=0.7822x R2=0.969
CoO 0%
CoO 2%
CoO 5%

b

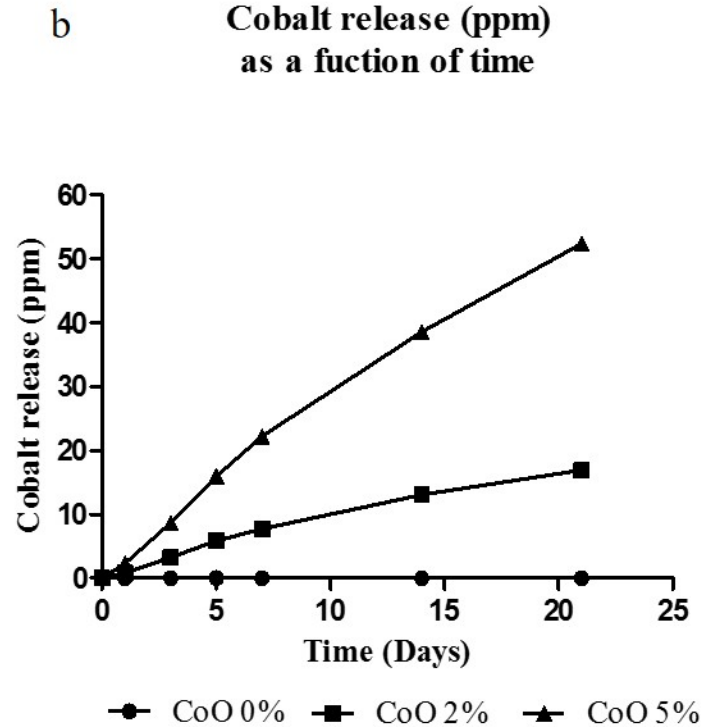
Cobalt release (ppm) as a fuction of time
Cobalt release (ppm)
Time (Days)
CoO 0%
CoO 2%
CoO 5%

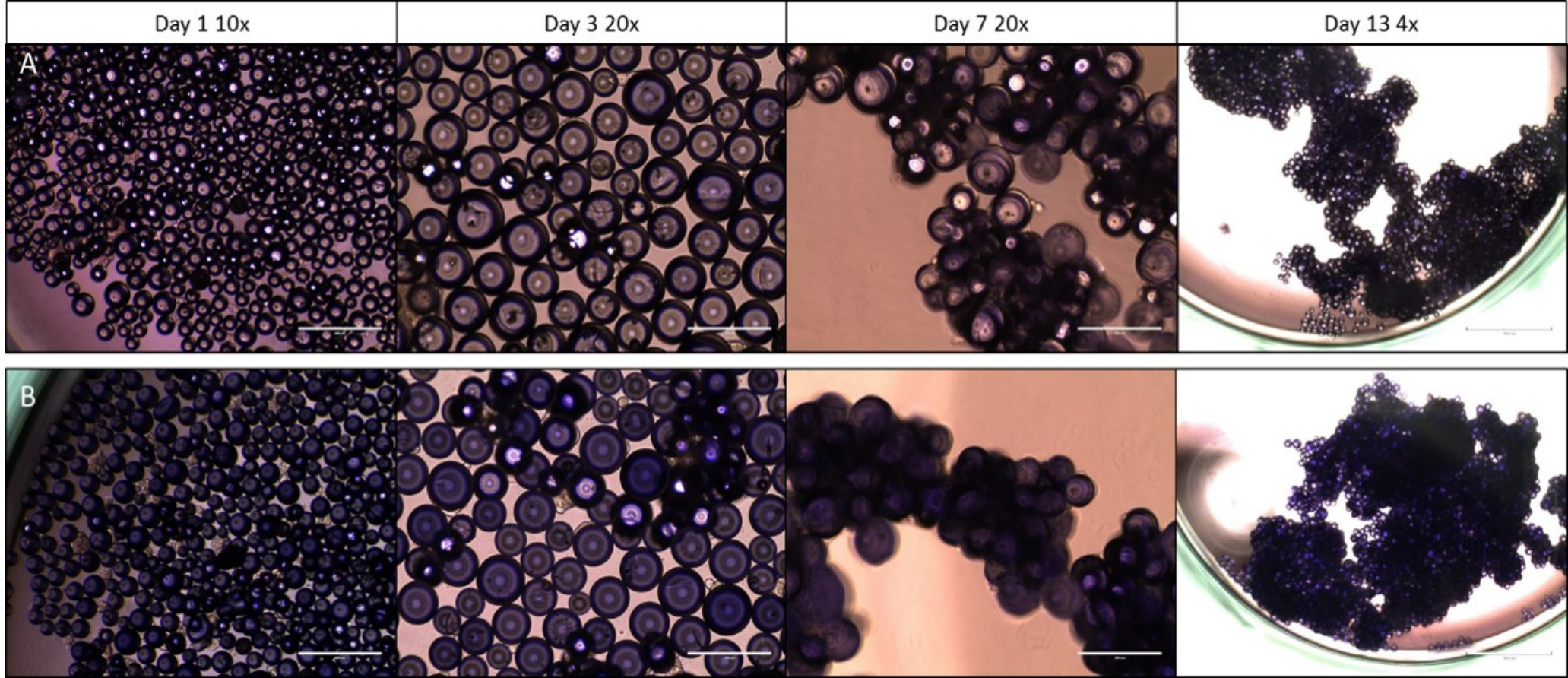
Day 1 10x
Day 3 20x
Day 7 20x
Day 13 4x
A
B

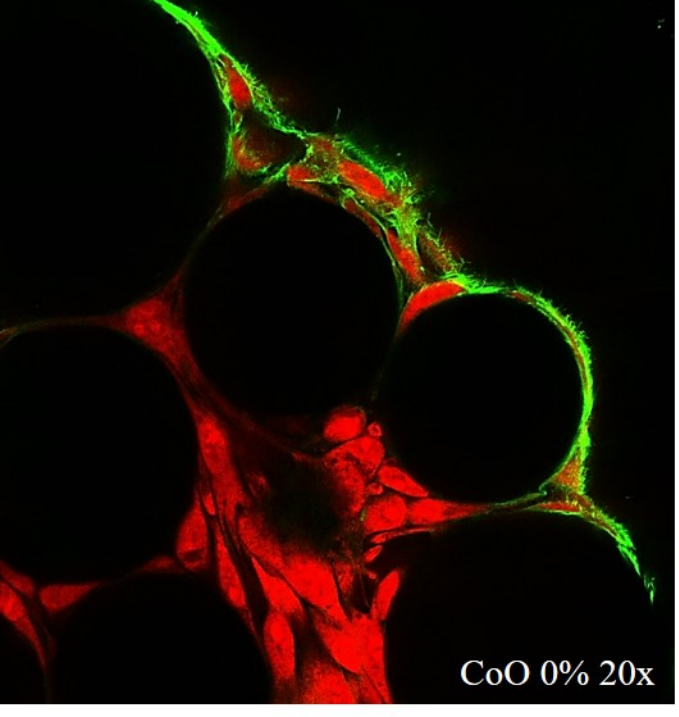
CoO 0% 20x

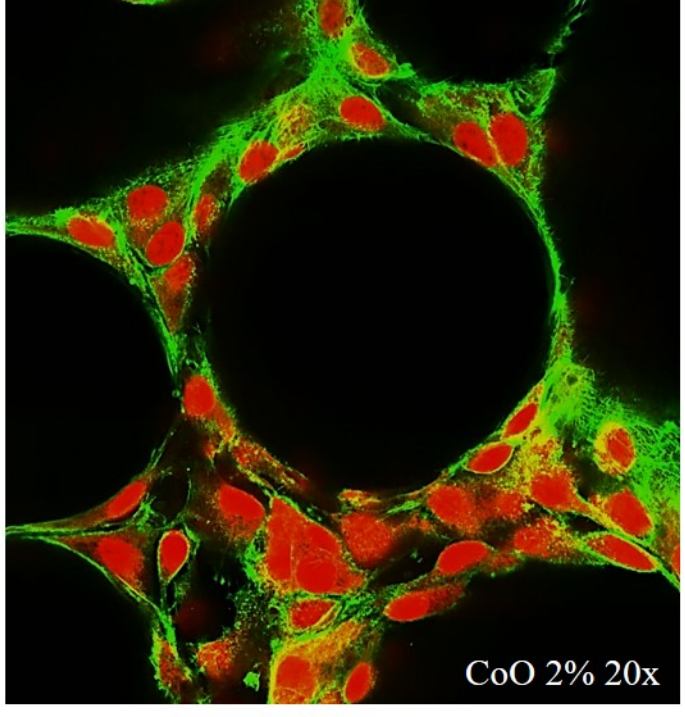
CoO 2% 20x

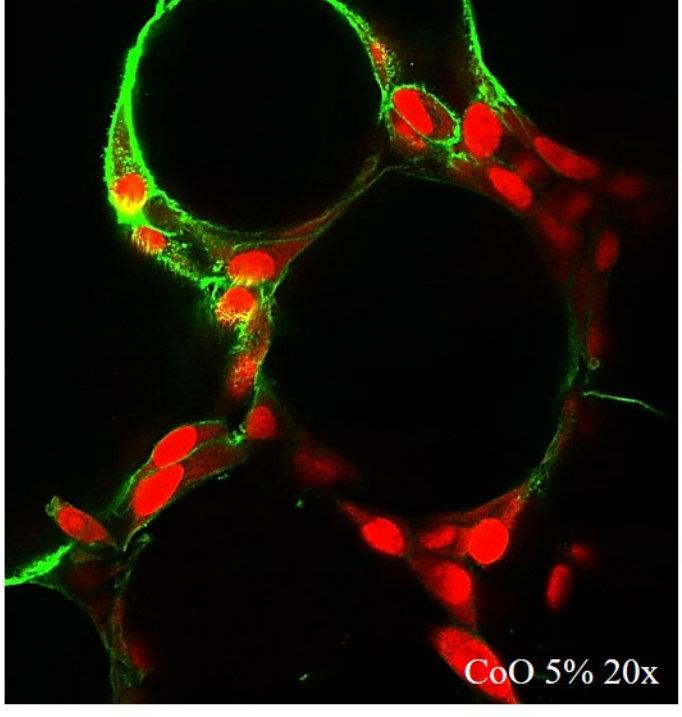
CoO 5% 20x

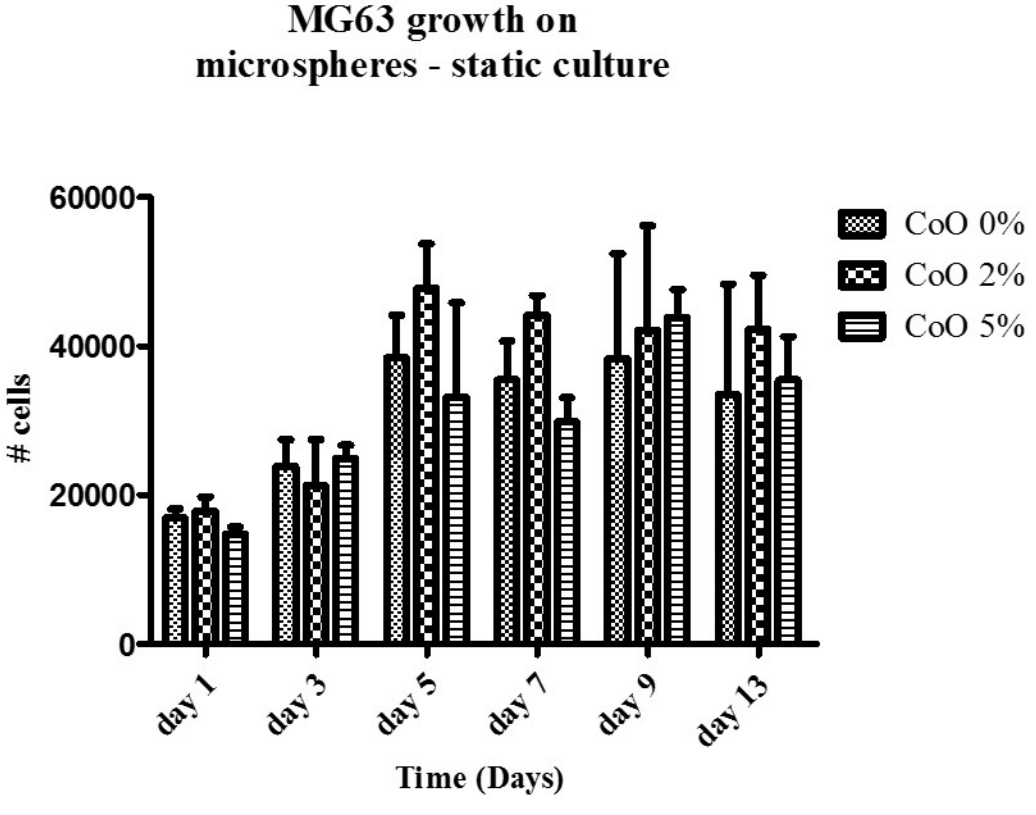
MG63 growth on microspheres - static culture
60000
40000
20000
0
cells
CoO 0%
CoO 2%
CoO 5%
day 1
day 3
day 5
day 7
day 9
day 13
Time (Days)

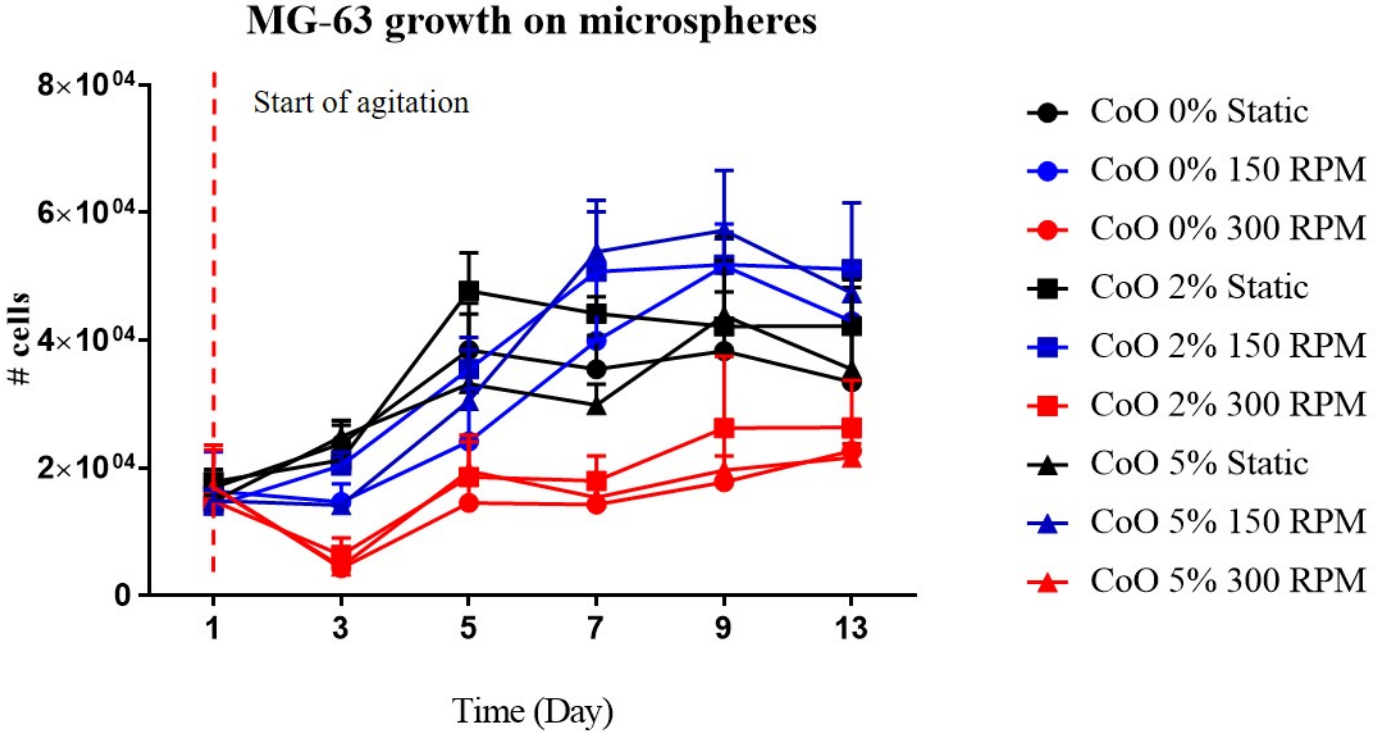
MG-63 growth on microspheres
Start of agitation
8×10^04
6×10^04
4×10^04
2×10^04
0
cells
1
3
5
7
9
13
Time (Day)
CoO 0% Static
CoO 0% 150 RPM
CoO 0% 300 RPM
CoO 2% Static
CoO 2% 150 RPM
CoO 2% 300 RPM
CoO 5% Static
CoO 5% 150 RPM
CoO 5% 300 RPM

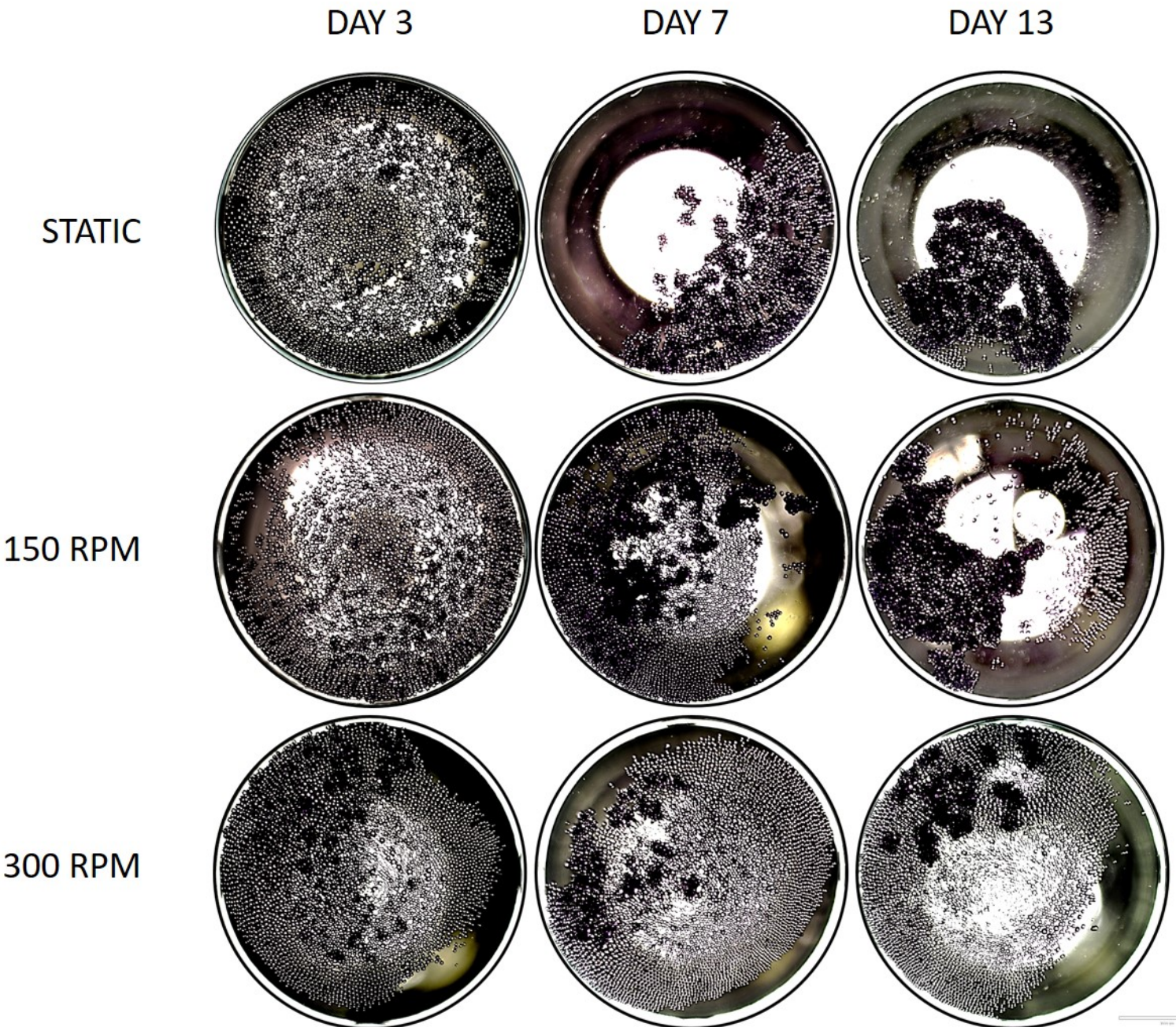
DAY 3
DAY 7
DAY 13
STATIC
150 RPM
300 RPM

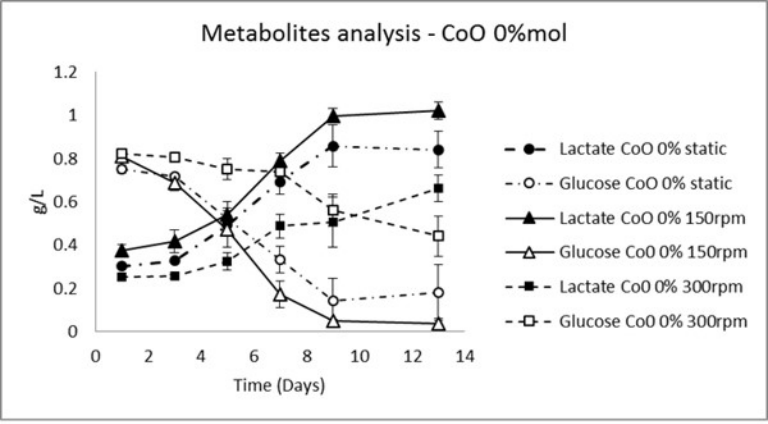
Metabolites analysis - CoO 0%mol
g/L
Time (Days)
Lactate CoO 0% static
Glucose CoO 0% static
Lactate CoO 0% 150rpm
Glucose Co0 0% 150rpm
Lactate Co0 0% 300rpm
Glucose Co0 0% 300rpm

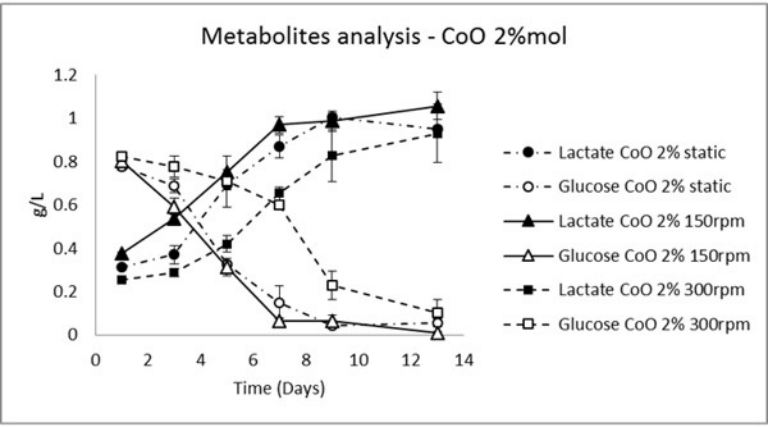
Metabolites analysis - CoO 2%mol
g/L
Time (Days)
Lactate CoO 2% static
Glucose CoO 2% static
Lactate CoO 2% 150rpm
Glucose CoO 2% 150rpm
Lactate CoO 2% 300rpm
Glucose CoO 2% 300rpm

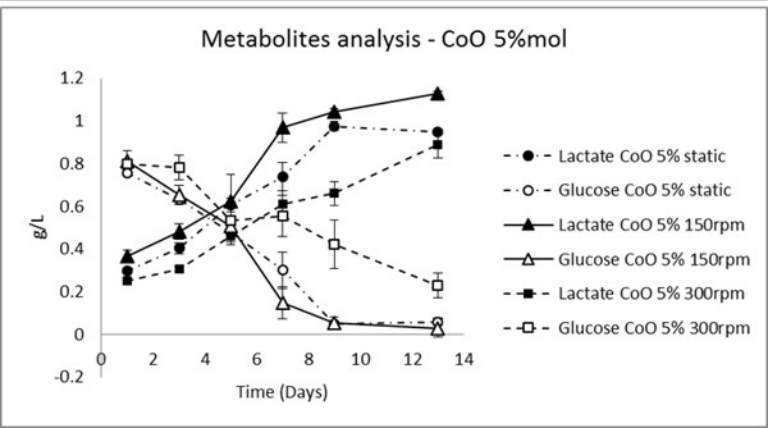
Metabolites analysis - CoO 5%mol
g/L
Time (Days)
Lactate CoO 5% static
Glucose CoO 5% static
Lactate CoO 5% 150rpm
Glucose CoO 5% 150rpm
Lactate CoO 5% 300rpm
Glucose CoO 5% 300rpm

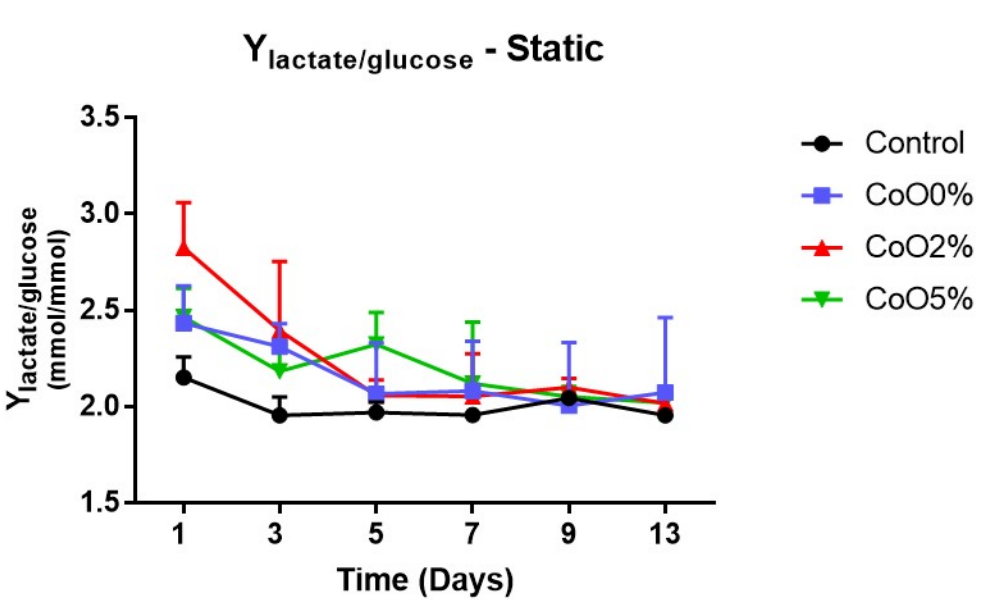
Y lactate/glucose - Static
Y lactate/glucose (mmol/mmol)
3.5
3.0
2.5
2.0
1.5
1
3
5
7
9
13
Time (Days)
Control
CoO0%
CoO2%
CoO5%

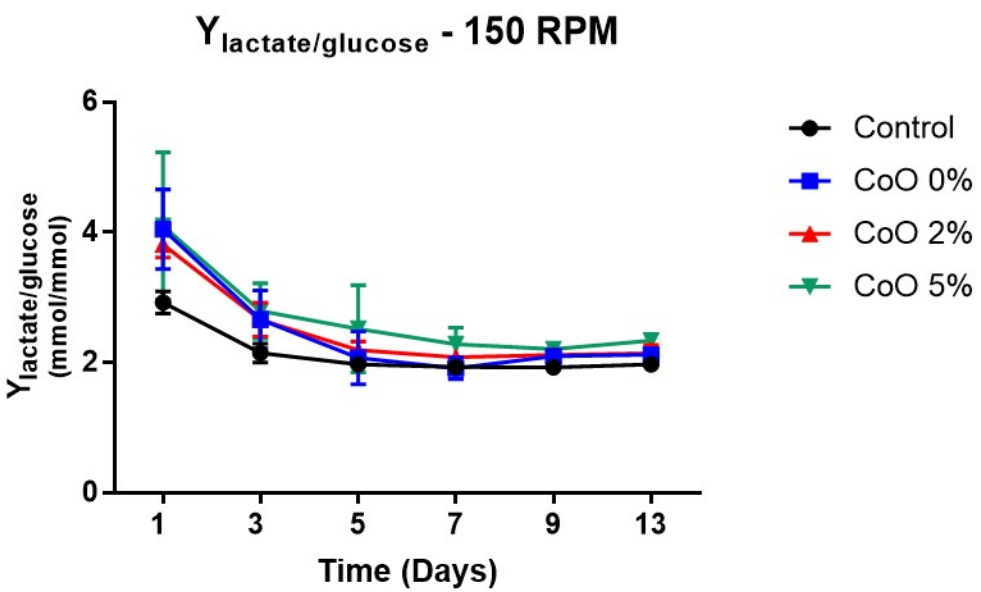
Y lactate/glucose - 150 RPM
Y lactate/glucose (mmol/mmol)
6
4
2
0
1
3
5
7
9
13
Time (Days)
Control
CoO 0%
CoO 2%
CoO 5%

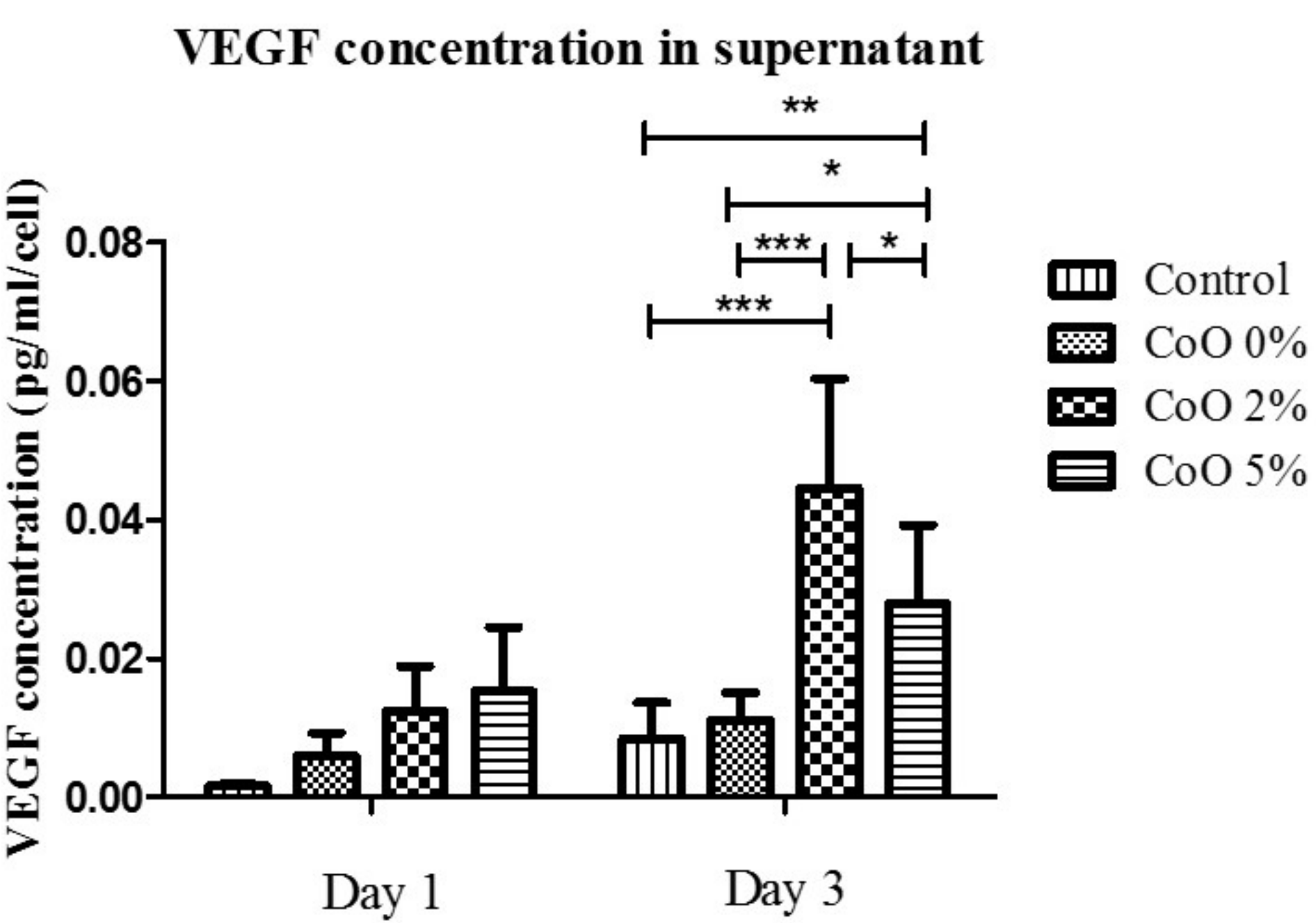
VEGF concentration in supernatant
VEGF concentration (pg/ml/cell)
0.08
0.06
0.04
0.02
0.00
**
*
***
*
***
Control
CoO 0%
CoO 2%
CoO 5%
Day 1
Day 3

	T_g (°C)	T_{c1} (°C)	T_{c2} (°C)	T_m (°C)
CoO 0%	415.4	588.3	677.0	729.3
CoO 2%	415.8	581.8	676.2	723.2
CoO 5%	416.2	586.2	678.5	713.2

Table A.1: Summary of glass transition temperature (T_g), crystallization temperatures (T_{c1} and T_{c2}) and melting temperature (T_m) for phosphate glass containing 0%, 2% and 5% mol CoO.

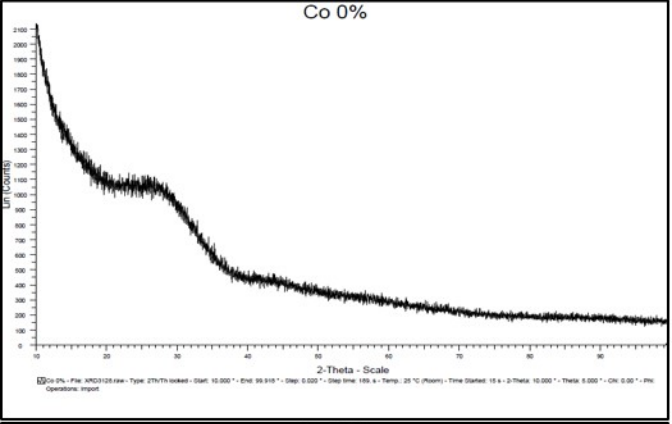
Co 0%
Lin (Counts)
2-Theta - Scale

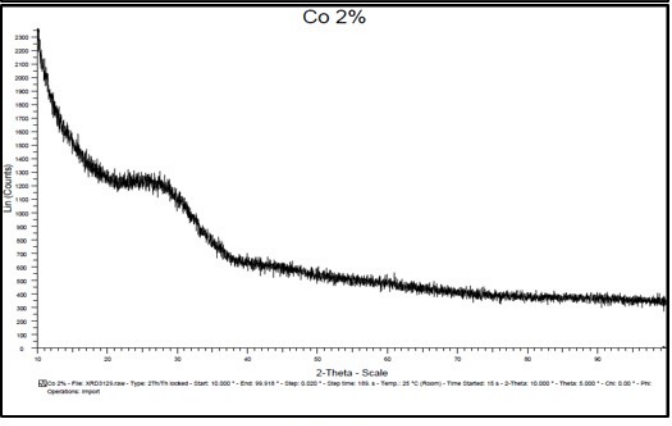
Co 2%
Lin (Counts)
2-Theta - Scale

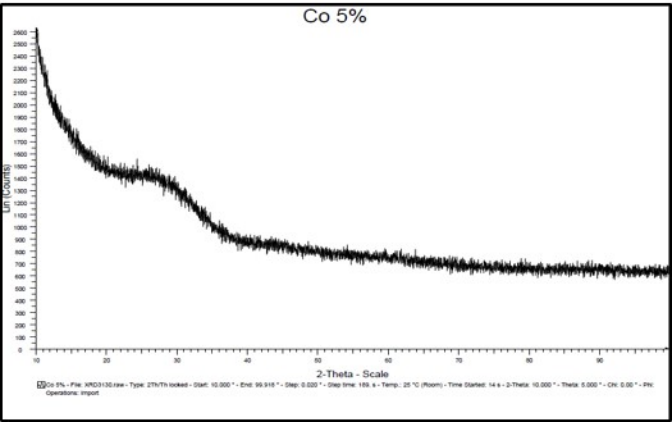
Co 5%
Lin (Counts)
2-Theta - Scale

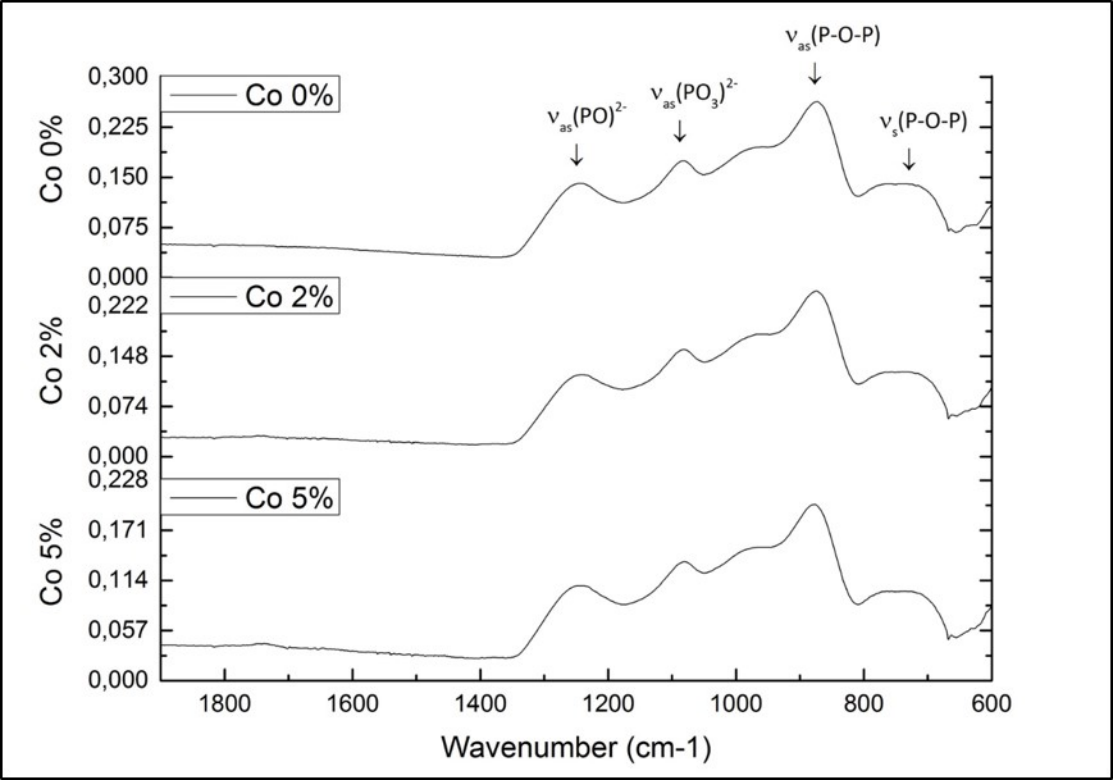
Co 0%
Co 2%
Co 5%
$\nu_{as}(PO)^{2-}$
$\nu_{as}(PO_3)^{2-}$
ν_{as}(P-O-P)
ν_s(P-O-P)
0,300
0,225
0,150
0,075
0,000
0,222
0,148
0,074
0,000
0,228
0,171
0,114
0,057
0,000
1800
1600
1400
1200
1000
800
600
Wavenumber (cm-1)

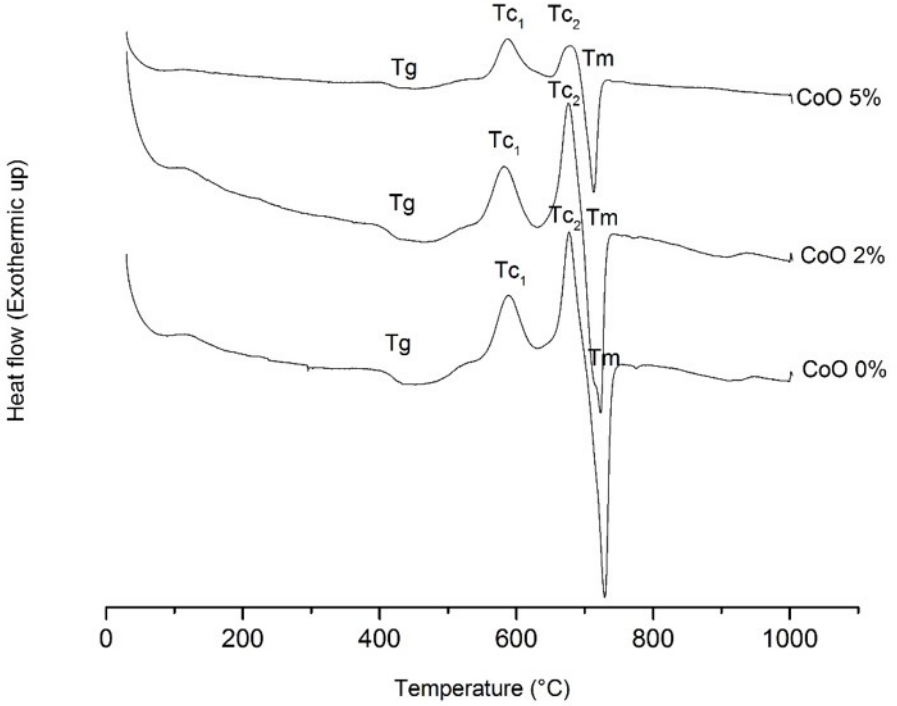
Tc1
Tc2
Tg
Tm
CoO 5%
Tc2
Tc1
Tg
Tc2
Tm
CoO 2%
Tc1
Tg
Tm
CoO 0%
Heat flow (Exothermic up)
0
200
400
600
800
1000
Temperature (°C)